The Astrophysical Journal, 834:129 (13pp), 2017 January 10 doi:10.3847/1538-4357/834/2/129

SEARCHING FOR BINARY SUPERMASSIVE BLACK HOLES VIA VARIABLE BROAD EMISSION LINE SHIFTS: LOW BINARY FRACTION

Lile Wang[1], Jenny E. Greene[1], Wenhua Ju[1], Roman R. Rafikov[2], John J. Ruan[3], and Donald P. Schneider[4,5]
[1] Princeton University Observatory, Princeton, NJ 08544, USA
[2] Institute for Advanced Study, Einstein Drive, Princeton, NJ 08540, USA
[3] Department of Astronomy, University of Washington, Box 351580, Seattle, WA 98195, USA
[4] Department of Astronomy and Astrophysics, The Pennsylvania State University, University Park, PA 16802, USA
[5] Institute for Gravitation and the Cosmos, The Pennsylvania State University, University Park, PA 16802, USA
Received 2016 May 19; revised 2016 October 31; accepted 2016 November 11; published 2017 January 9

ABSTRACT

Supermassive black hole binaries (SMBHs) are expected to result from galaxy mergers, and thus are natural byproducts (and probes) of hierarchical structure formation in the universe. They are also the primary expected source of low-frequency gravitational wave emission. We search for binary BHs using time-variable velocity shifts in broad Mg II emission lines of quasars with multi-epoch observations. First, we inspect velocity shifts of the binary SMBH candidates identified in Ju et al., using Sloan Digital Sky Survey spectra with an additional epoch of data that lengthens the typical baseline to ∼10 yr. We find variations in the line of sight velocity shifts over 10 yr that are comparable to the shifts observed over 1–2 yr, ruling out the binary model for the bulk of our candidates. We then analyze 1438 objects with eight-year median time baselines, from which we would expect to see velocity shifts $>1000\,\mathrm{km\,s^{-1}}$ from sub-parsec binaries. We find only one object with an outlying velocity of $448\,\mathrm{km\,s^{-1}}$, indicating—based on our modeling—that $\lesssim$1% (the value varies with different assumptions) of SMBHs that are active as quasars reside in binaries with ∼0.1 pc separations. Binaries either sweep rapidly through these small separations or stall at larger radii.

Key words: accretion, accretion disks – galaxies: active – galaxies: nuclei – quasars: emission lines – quasars: general

1. INTRODUCTION

The mergers of supermassive black holes (SMBHs) likely play a key role in SMBH formation and massive galaxy evolution (e.g., Barnes & Hernquist 1992; Volonteri et al. 2003a, 2003b; Springel et al. 2005). Because most massive galaxies harbor SMBHs at their centers (see Kormendy & Ho 2013, and references therein), and galaxies grow via hierarchical mergers, we expect binary SMBHs to form, but we have no empirical constraints on the rate of merging of these binary systems. As the most intense sources of spacetime curvature, merging BHs are expected to be a dominant source of gravitational radiation at low frequency (e.g., Abadie et al. 2011; Amaro-Seoane et al. 2013), dominating the low-frequency gravitational wave background (GWB; e.g., Phinney 2001; Ravi et al. 2015). The merger rate also has important implications for the spin distribution of SMBHs (e.g., Barausse & Rezzolla 2009; Gergely & Biermann 2012; Hofmann et al. 2016).

The typical SMBH merger scenario consists of several phases of evolution (e.g., Begelman et al. 1980). At large radius (kpc scales), the SMBHs dissipate energy and angular momentum by dynamical friction with stars in galactic bulges, until the binary hardens and reaches an orbital velocity that is greater than the typical velocity dispersion of the bulge stars (e.g., Quinlan 1996; Merritt & Milosavljević 2005). At these ∼ parsec separations, in an axisymmetric system, there are no longer sufficient stars to be scattered by the SMBH binary. Gravitational wave emission cannot efficiently facilitate the merger of BH binaries until $\lesssim 10^{-3}$ pc scales (see also Begelman et al. 1980). In principle, the SMBH binary may stall at ∼1 pc indefinitely, a possibility known as the "final parsec" problem (e.g., Begelman et al. 1980). Many solutions have been proposed to efficiently merge SMBH binaries within a Hubble time, including a gas-assisted inspiral model (e.g., Ivanov et al. 1999; Haiman et al. 2009; Rafikov 2013; Gold et al. 2014; Ivanov et al. 2015; Rafikov 2016), or enhanced efficiency of binary-star scattering in triaxial halos (Khan et al. 2012; Vasiliev et al. 2015; Khan et al. 2016). However, from both observational and theoretical perspectives, it remains unclear whether SMBH binaries merge efficiently or stall forever.

The goal of the current work is to statistically constrain the duration of the SMBH binary phase at ∼0.1 pc scales, by searching a large population of quasars, using multi-epoch spectroscopy, for time-varying radial velocity shifts caused by the binary orbital motion. A handful of studies have attempted to image SMBH binaries using radio observations (Rodriguez et al. 2006; Burke-Spolaor 2011), but in general it is prohibitive to spatially resolve such binaries at cosmological redshifts where the cosmic mass density in BHs is built up. Therefore, time-domain searches are required. One approach is to use light-curves to search for quasi-periodic variability caused by interaction of the circumbinary disk with the SMBH binary (e.g., Valtonen et al. 2008; Charisi et al. 2015; Graham et al. 2015a, 2015b). Here, we focus on time-resolved UV spectroscopy.

Two spectroscopic techniques have been employed to identify possible SMBH binaries. One class of methods measures the "absolute" shifts of the broad emission lines (BELs), thought to be produced close to the black holes, relative to the narrow emission lines, which are believed to have redshifts close to that of the host galaxy (e.g., Boroson & Lauer 2009; Decarli et al. 2010; Tsalmantza et al. 2011; Eracleous et al. 2012). This method tends to select a very rare sub-class of targets with large velocity offsets in the BELs.

Such an appearance may well result from the orbital motion; however, in many cases, they may be produced by alternative mechanisms (e.g., Gezari 2005; Eracleous et al. 2012; Steinhardt et al. 2012). To resolve this ambiguity requires a long baseline of observations. In addition, many of these objects exhibit variations in their BEL line shapes as the luminosity varies (e.g., Decarli et al. 2013), which may contaminate the velocity shift detections. A related method uses binary BH models to predict kinematic signatures of binarity in the broad lines (see Nguyen & Bogdanović 2016).

The second type of search, utilized in this paper (see also Ju et al. 2013; Shen et al. 2013), employs multiple observations of the same quasar to search for time-varying velocity shifts that may indicate orbital motion. We focus here on $0.4 < z < 2$ quasars, and use the Mg II $\lambda 2800$ Å line to trace the BEL region.

1.1. The Method

Our basic binary BH search approach is to cross-correlate multiple epochs of spectroscopic observations of the same objects in search of radial velocity shifts that might indicate binary orbital motion (see, e.g., Gaskell 1983; Simić & Popović 2016). We measure the velocity shift ΔV between epochs with typical time-baselines ranging from 1 to 14 years, and then attempt to ascertain, using multiple epochs, whether ΔV can be ascribed to orbital motion. Thus, we are using the broad-line region (BLR) of these quasars as the dynamical tracer. This method has both strengths and weaknesses that set some fundamental limitations on what we can do.

The main strength is that we can target a large number of accreting BHs at a cosmologically interesting time ($z \approx 2$), when merging activity peaked. Because there are very few concrete observational limits on the lifetimes of binary BHs, any tool that might yield interesting limits must be explored.

The weakness is that we are depending on BLR physics that we do not understand. There are a number of uncertainties that we must keep in mind as we evaluate the observational results. First of all, we do not know the size of the BLR precisely. At the point where the BLR is no longer gravitationally bound to an individual BH, but rather envelops both, our method no longer works. Here, we assume that relationships between BLR size and AGN luminosity that have been calibrated at lower redshift also apply to these moderate redshift quasars, even if they harbor binary BHs. Generally speaking, the BLR size is likely 0.01–0.1 pc for the quasars that we consider here (Shen & Loeb 2010). Thus, we can only hope to probe binaries with separations comparable to or larger than a tenth of a pc. At larger separations, we do not have long enough time baselines to be sensitive to orbital velocity shifts. At smaller separations, the two BHs will likely share a common BLR.

There is also the possibility that the BLR is completely different in the case of binary BHs. There may be suppressed accretion, different dynamics in the BLR due to tidal truncation, or even no accretion at all on sub-parsec scales. If the BLR is different, then our BH scaling relations, which already carry large systematic uncertainty (e.g., Shen et al. 2013), may be even more uncertain. Therefore, we adopt a range of reasonable values for $R_{\rm BLR}$ throughout the paper, to reflect these uncertainties. If accretion is considerably lowered, then our method has limited value. Still, given the lack of observational constraints on SMBH binary evolution timescales, it is worth searching for large radial velocity shifts in the data.

The second uncertainty that we must contend with is that BLRs may vary in velocity even in single AGN (Sredzinska et al. 2016). In some dramatic cases, these shifts are believed to arise from hot spots in the accretion disk (e.g., Eracleous et al. 1997). Even in typical AGN, velocity shifts can arise as the AGN continuum varies, depending on the illumination pattern of the BLR (Barth et al. 2015, and discussion in Section 3.4). We do not know the full range of velocities that may arise from this reverberation. Therefore, these velocity shifts comprise a significant source of noise for our method.

In Ju et al. (2013), we found that the distribution in ΔV for two epochs, with $\sim$1 year time separations, had a width of $82\,{\rm km\,s^{-1}}$, and this width is very likely dominated by line variability in AGN with single BHs that leads to measured velocity shifts, but is unrelated to orbital motion. Because we do not know the full distribution of velocity shifts in single AGN as a function of time, we must try to empirically determine this distribution from the data we have at hand, which we will discuss in Sections 5 and 6. It is important to understand from the beginning that spectral variability in the lines of single AGN constitutes a serious source of contamination for us. On the other hand, as we will show from our data, velocity shifts of $\Delta V > 1000\,{\rm km\,s^{-1}}$ seem to be very rare from a single AGN. Given the 10-year time baselines considered here, we would be able to detect such dramatic velocity offsets from radial velocity shifts in binary BHs. Thus, we can draw some conclusions about the residence times of binary BHs from these data despite contamination from single AGNs.

1.2. Structure of the Paper

Our paper is slightly non-standard in that we present two related (but distinct) experiments. First, in Section 3 we present a third spectroscopic epoch for 21 candidate binary BHs from Ju et al. (2013). Compared to this work, we increase the time baseline of monitoring by an order of magnitude. This first experiment highlights very well how velocity jitter in the BLRs of single BHs acts as a major source of contamination for our method. In the short term, we are forced to search for only the most extreme velocity shifts that may result from long time-baseline monitoring.

Second, in Section 4, we take advantage of considerably more data from the Sloan Digital Sky Survey (SDSS) III/BOSS survey, which allows us to expand on the original work of Ju et al. (2013) by adding a number of new objects. In particular, we are able to consider $\sim$10 year time baselines for 10,121 quasars in total (1438 with high signal-to-noise ratio (S/N), see Section 4). With such long time baselines, we can focus on the expected tail of $\Delta V > 1000\,{\rm km\,s^{-1}}$ objects expected from orbital motion.

The remainder of the paper is structured as follows. Section 2 explains the method we use for data analysis. The results of our two experiments are interpreted in Section 5. Section 6 discusses our findings and summarizes the paper.

2. CROSS-CORRELATION ANALYSIS

For both parts of our paper, our main method is to cross-correlate multiple epochs of spectroscopy in search of radial velocity shifts. Here, we describe our main steps in performing the cross-correlation. We implement our analysis routines in

Table 1
Emission Line Masks for Continuum Fitting

Species	Line Center (λ_c/Å)	Half-width (λ_w/Å)
O VI	1035	35
Lyα	1216	75
N V	1241	35
Si IV	1398	35
C IV	1549	35
He II	1640	35
C III	1909	35
Mg II	2799	80
O II	3727	35
Hδ	4102	80
Hγ	4340	80
O III	4363	35
Hβ	4861	100
O III	4959	35
O III	5007	35
O I	6350	35
O I	6364	35
N II	6548	35
Hα	6563	330
N II	6583	35
S II	6716	35
S II	6734	35

`Python`, and make use of the least-squares fitting package with the Levenberg–Marquardt algorithm, `lmfit`, wherever fitting is needed. To detect velocity shifts, we focus on the temporal variations of BELs. We describe here the analysis we perform to prepare the spectra for cross-calibration.

2.1. Fitting and Subtraction of the Continuum Emission

Similar to Ju et al. (2013), we first fit the continuum emission and remove it. Continuum subtraction is needed because either intrinsic variability in the continuum shape or artifacts in the continuum between epochs can contaminate the cross-correlation signal. We list the significant emission lines that affect our continuum fitting process in Table 1. Wavelength ranges centered at λ_c with half-width λ_w are masked. After this procedure, the continuum emission is fitted by a fifth-order polynomial, which empirically allows for sufficient flexibility. This continuum-removal procedure isolates the BEL from the quasar continuum. We note that all broad lines, including the Fe II pseudocontinuum, provide signal that—in principle—should trace the radial velocity motions of the BLR. Thus, we do *not* fit and remove the broad Fe lines.

After removal of the continuum, we extract the Mg II BEL feature from the spectrum in the rest-frame wavelength window (2698 Å $< \lambda <$ 2798 Å or 2748 Å $< \lambda <$ 2848 Å). The spectrum of each object is converted into the rest frame using the redshift value of the first epoch observation, because there is significant variance between the redshift measurements for different epochs: the mean and standard deviation of $(z_{\rm DR7} - z_{\rm DR12})$ are 0.00032 and 0.068, respectively. Discrepant redshift data are indications of the quasars' intrinsic variations. By using the redshift of the first epochs uniformly, we are able to measure any radial velocity shifts without additional noise from the redshift measurements.

2.2. Cross-correlation Identification of Velocity Shifts

Taking the continuum-subtracted spectra as input, we now evaluate the cross-correlation function between the spectra with the maximum time separation. We evaluate the normalized cross-correlation function, using the following formula (e.g., Ju et al. 2013):

$$\mathrm{Corr}(D) = \left[\sum_{i=0}^{N}(a_i - \bar{a})^2\right]^{-1/2}\left[\sum_{i=0}^{N}(b_i - \bar{b})^2\right]^{-1/2} \times \left[\sum_{i=0}^{N-|D|+1}(a_{i+D} - \bar{a})(b_i - \bar{b})\right], \quad (1)$$

where D is the number of "delayed" channels, and a_i and b_i are the measured spectral fluxes from the two epochs of observation of the ith channel. The SDSS and BOSS spectrographs are different (see Smee et al. 2013), and we interpolated the DR12 spectra onto the channel grid of DR7 spectra to conduct sensible correlation calculations. The value of Corr(D) peaks at $D = 0$ when the two spectra are identical. Results of these cross-correlation procedures are illustrated by, as an example, Figure 1.

Before feeding the spectra into Equation (1), we "oversample" the original spectrum by a factor of 8. This procedure does not introduce any extra information, but it makes the correlation function smoother and eases the peak-finding procedure. The velocity shift represented by each oversampled channel (i.e., the resolution of our cross-correlation scheme) is $\delta v_{\rm res} = 8.6\,{\rm km\,s^{-1}}$.

In general, because the Mg II lines are smooth and broad, we expect the cross-correlation function to be dominated by a single peak. Exceptions are produced by broad absorption lines (Lundgren et al. 2007; Gibson et al. 2008, 2010), but we have removed these features by hand. Other small bumps may be caused by narrow absorption lines or noise features, but they do not impact our ability to identify the primary cross-correlation peak.

We aim to find the maximum in the *overall* structure of the correlation function. This is different from Ju et al. (2013), in which the authors used a somewhat smaller window to determine the cross correlation maximum. By trial and error, we found that using the sum of three models to fit the maximum works best. We fit the cross-correlation function with a combination of two skewed Gaussian models (with positive-definite amplitude, providing skewness to our fitting function), and a second-order polynomial to the residual continuum. It is straightforward to identify the maximum of the cross-correlation signal using the fit. The location of the fit maximum, $\Delta\lambda$, is directly used to calculate the value of the velocity shift,

$$\Delta V \simeq \frac{\Delta\lambda}{\lambda_{\rm Mg\,II}}c, \quad (2)$$

where c is the speed of light.

3. EXPERIMENT 1: JU ET AL. FOLLOW-UP

3.1. Sample Properties

Ju et al. (2013) analyzed 4024 QSOs with two epochs of observation in the quasar catalog of the seventh data release (DR7) of SDSS (York et al. 2000; Schneider et al. 2010). For

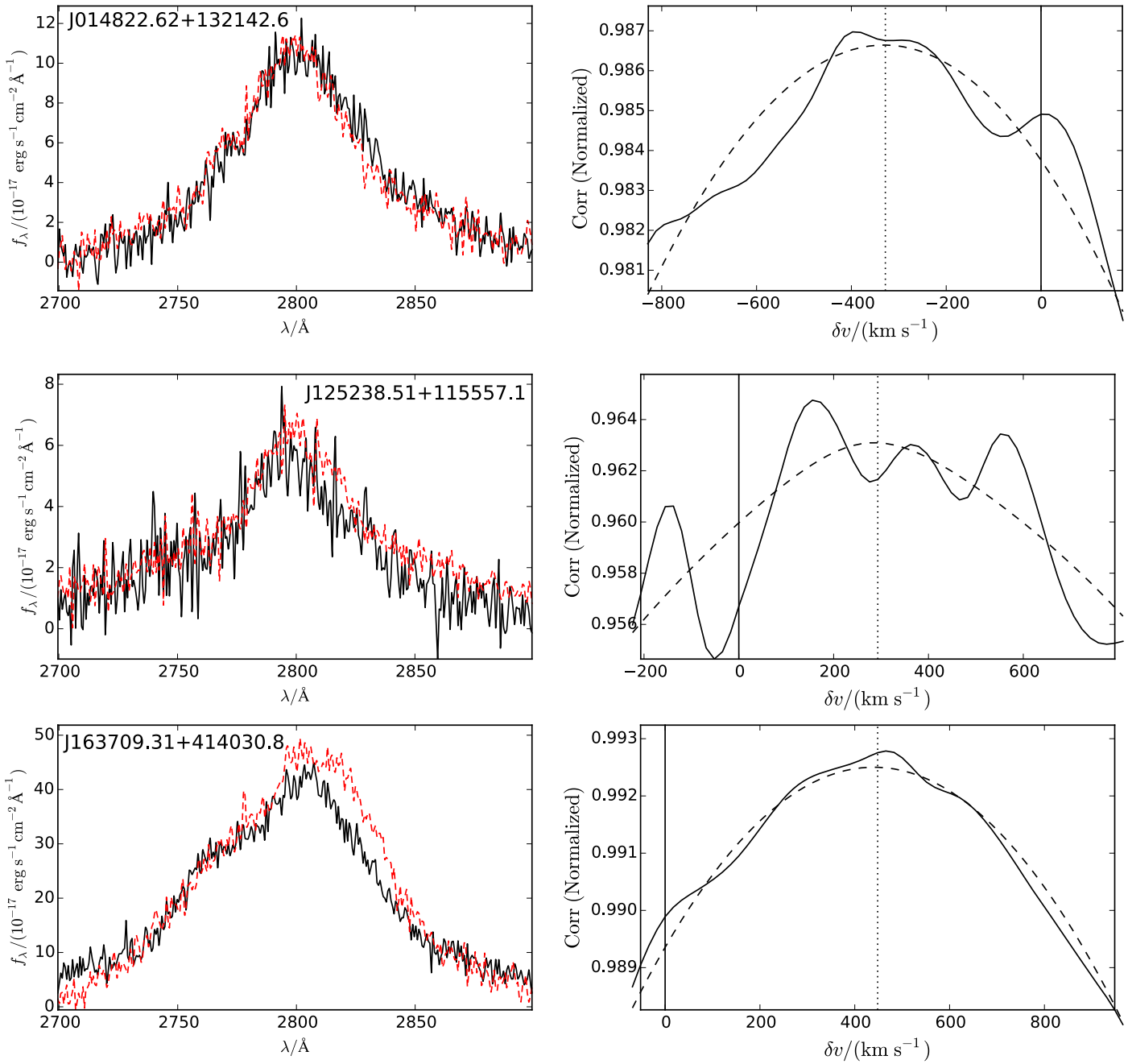

Figure 1. Examples of the cross-correlation between two epochs of spectra of the Mg II line, showing three of the candidates with the most prominent line shifts (see Table 3): J014822.62+132142.6 (top row), J125238.51+115557.1 (middle row), and J163709.31+414030.8 (bottom row). Left column: comparison of spectra. The black lines represent the observation of the first epoch, and the red dashed lines represent the second. Right column: the cross-correlation function (see Equation (1)). The solid curve shows results directly measured from the spectra, whereas the dashed curve is the result using Gaussian fitting. The maximum of the fitted curve is indicated by a vertical dotted line, and $\delta v = 0$ is indicated by a vertical solid line.

completeness, because this paper analyzes additional observations of their targets, here we briefly summarize their final sample selection.

In order to focus on the Mg II emission line, objects were selected in the redshift range $0.36 < z < 2.0$, with g-band absolute PSF magnitudes ranging from -18.4 to -27.5 mag (median -24.1 mag). The typical time lag between observations ranged from 0.003 to 7.03 year, with mean value 0.7 year. Based on BEL scalings (Shen et al. 2011), the virial BH masses range from $10^7\,M_\odot$ through $10^{10.5}\,M_\odot$ (peaked at $10^{8.65}\,M_\odot$). Ju et al. (2013) focused on the 1523 objects with high S/N (S/N pixel^{-1} > 10; each pixel corresponds to 70 km s^{-1}).

Using a cross-correlation between the two epochs (see Section 2.2 below), the distribution of velocity shifts was measured first for all objects, regardless of time separation, and found to have a dispersion of $\sigma = 101$ km s^{-1} for the whole sample, and $\sigma = 82$ km s^{-1} for the high S/N pixel^{-1} subsample. Just requiring velocity shifts greater than $>3\sigma$ yielded 7 high-confidence candidates, and 64 extra possible candidates.

Twenty-one of these candidates were revisited as part of the Time-Domain Spectroscopic Survey (a part of SDSS III), which provides spectroscopic data for time-variable objects, including roughly 135,000 quasars (see Morganson et al. 2015; Myers et al. 2015; Ruan et al. 2016). With this additional

epoch, we now have much longer observed time baselines for these objects, ranging from 12.91 through 14.31 year (median 14.16 year), compared to the original 0.17 year to 6.16 year (median 0.98 year). Furthermore, we now have a total of three epochs. These observations not only yield more reliable velocity shift detections by probing longer timescales, but also trace the evolution of these systems in order to address whether the velocity shifts that were detected in Ju et al. (2013) are consistent with the binary BH picture.

3.2. Verification Criteria

The data analysis algorithm described in Section 2 is different from the method presented in Ju et al. (2013), although the two are closely related. To be sure that we can analyze all three epochs consistently, we first apply our analysis routines to the two-epoch spectra that were examined in Ju et al. (2013) to verify that the velocity shifts are detected with similar values. Focusing on the selected candidates specified in Ju et al. (2013), we analyzed the spectral data acquired during the first two epochs using the procedures described in Sections 2.1 and 2.2, and reproduced the Ju et al. (2013) $|\Delta V|$ measurements consistently. As a sanity check, we re-apply our scheme to the candidates in Ju et al. (2013) and find that they all remain candidate binaries under this new algorithm.

As an additional sanity check, in addition to Mg II, we also examine velocity shifts measured with the Hβ BEL if applicable. We exclude those with S/N pixel^{-1} < 1 in the wavelength window surrounding Hβ BEL (see Section 4 for the definition of S/N pixel^{-1}). Hβ does come with additional complications due to the blending of [O III]$\lambda\lambda$4959, 5007. Values of ΔV measured by Hβ and Mg II do exhibit some level of consistency, but the Hβ results still suffer from considerable uncertainties due to blending with narrow lines, causing a good deal of scatter between the two estimates.

3.3. The Additional Epoch

After analyzing the first two epochs consistently, we now turn to the third epoch. For the follow-up observations, we use a straightforward criterion to determine whether the original velocity shift can be ascribed to orbital motion. For a secondary SMBH in a binary system, we define the empirical acceleration along the line of sight (LoS) $a_{\rm LoS}$,

$$a_{\rm LoS} \equiv \frac{\Delta V}{\Delta t} = \frac{\Delta V}{(1+z)\Delta\tau}, \quad (3)$$

where Δt is the time baseline in the observer's rest frame, and $\Delta\tau$ is its counterpart in the rest frame of the object. In what follows, we will use t for the time variable in the observer's frame and τ for time in object's frame. This "acceleration" magnitude should not be thought of as a physical quantity, because ΔV is measured in the rest frame of the object, but simply as a convenient way to test the consistency of the different epochs.

The typical timescale of variation is evaluated, regarding the time variability of $a_{\rm LoS}$ and ΔV. We assume that the secondary (the smaller BH mass in the binary system) carries the BLR, and that the virial mass inferred from the BEL width indicates the mass of the secondary. Hence, in what follows, we use $M_{\rm BH}$ to denote the mass of secondary. We also assume that the secondary travels along a circular orbit by $\pi/2$ phase (which covers a full amplitude of LoS motion). Considering time dilation, the time it takes the binary to cover a quarter of its orbit is

$$\Delta t_a = \frac{\pi(1+z)}{2\Omega} = 23.4\ \text{year} \times (1+z)\left(\frac{M_{\rm BH}/q}{10^9\,M_\odot}\right)^{-1/2}\left(\frac{r}{0.1\ \text{pc}}\right)^{3/2}, \quad (4)$$

where Ω is the orbital angular speed assuming a circular orbit,

$$\Omega \equiv \left|\frac{GM_{\rm BH}(1+q)}{r^3 q}\right|^{1/2}, \quad (5)$$

and q is the mass ratio of the secondary to primary BH.

Our velocity shift detection time baseline is around $\Delta t \sim 10$ year. The separation r between the two BHs must be $\sim$0.1 pc or smaller to detect the velocity shifts in $\sim$1 year, as set by Ju et al. (2013). In that case, we would expect Δt_a to be comparable to Δt. We would also expect $a_{\rm LoS}$ to maintain a similar amplitude when we inspect the ensemble of binary system as a whole. Thus, a relatively steady value of $a_{\rm LoS}$ is the criterion that we adopt to determine whether the velocity shifts observed in Ju et al. (2013) can be attributed to binary orbital motion.

On the other hand, it is worth noting that orbital motion could significantly change the value, and even potentially the direction, of $a_{\rm LoS}$ for a BH binary with a high mass and a small orbital separation. Also, there may be cases where the velocity shift is significant during a short epoch, but small in the long run. Indeed, consider a BH binary on a circular orbit with initial orbital phase ϕ, angular speed Ω, orbital velocity $V_{\rm co}$, and inclination angle i. After a period of time Δt, the magnitude of velocity shift is

$$\frac{|\Delta V|}{\Delta\tau} = \frac{2V_{\rm co}}{\Delta\tau}\left|\sin\left(\phi+\frac{\Omega\Delta\tau}{2}\right)\sin\left(\frac{\Omega\Delta\tau}{2}\right)\sin i\right|. \quad (6)$$

Given a special initial phase ϕ and inclination angle i, the apparent acceleration can be as large as $\sim\Omega V_{\rm co}$ in the short term. As Δt increases, the value of acceleration will drop significantly, being no greater than $2V_{\rm co}/\Delta\tau$. However, we note that this will only happen under specific initial conditions, and cannot dominate the sample statistically.

3.4. Results

We measure the velocity shifts of the candidates from DR7, presented by Ju et al. (2013). Table 2 compares and updates the results for the Ju et al. (2013) objects using the SDSS IV spectra acquired for this purpose (Dawson et al. 2015). It is immediately clear that the velocity shifts are not consistent with our expectations for orbital motion. The inferred $a_{\rm LoS}$ values are lower than expected, often by an order of magnitude. The magnitude of the apparent acceleration is always decreasing over the longer time baseline. If the velocity shifts were due to orbital motion, one would expect to observe that a fraction of $a_{\rm LoS}$ measurements increase over time, which is not the case here.

Instead, we find comparable values of ΔV between the first and second epoch (typically separated by one year) and between the first and third epoch (typically separated by eight years). The correlation coefficients between the two different

Table 2
Follow-up Measurement of Velocity Shift

SDSS ID	z	Δt_0 (year)	ΔV_0 (km s^{-1})	$a_{\rm LoS,0}$ (km s^{-1} yr^{-1})	Δt_1 (year)	$\Delta V_{1,\rm Mg\,II}$ (km s^{-1})	$a_{\rm LoS,1,Mg\,II}$ (km s^{-1} yr^{-1})	$\Delta V_{1,\rm H\beta}$ (km s^{-1})	$a_{\rm LoS,1,H\beta}$ (km s^{-1} yr^{-1})
(1)	(2)	(3)	(4)	(5)	(6)	(7)	(8)	(9)	(10)
J002028.34+002915.0	1.93	0.2301	310	1347	14.15	−155.5	−11.0	⋯	⋯
J002311.06+003517.5	0.42	0.23	698	3035	14.15	181.0	12.8	⋯	⋯
J002411.66+004348.1	1.79	1.15	444	386	14.17	−51.8	−3.7	⋯	⋯
J002444.12+003221.2	0.40	0.23	380	1652	14.21	309.6	21.8	154.8	10.9
J003451.86–011125.6	1.84	1.28	−362	−283	14.28	−8.6	−0.6	⋯	⋯
J004052.15+000057.3	0.41	1.28	−1501	−1173	14.31	112.1	7.8	293.1	20.5
J004918.98+002609.5	1.94	0.28	−290	−1036	14.26	−698.2	−49.0	⋯	⋯
J011310.39+003113.3	0.41	1.12	552	493	14.27	198.3	13.9	190.1	13.3
J013418.19+001536.7	0.40	1.05	−1863	−1774	14.22	103.7	7.3	0.0	0.0
J014209.72+002348.3	1.35	1.14	−414	−363	14.01	−34.6	−2.5	⋯	⋯
J014415.13+002349.7	1.71	1.14	345	303	14.01	146.5	10.5	⋯	⋯
J014905.16+005925.4	1.00	1.12	−299	−267	14.27	−414.7	−29.1	⋯	⋯
J015454.88+004043.8	1.65	0.9	670	744	14.06	60.3	4.3	⋯	⋯
J020527.77+005747.6	1.24	0.18	293	1628	14.10	34.6	2.5	⋯	⋯
J020646.97+001800.6	1.68	0.18	362	2011	14.18	−51.8	−3.7	⋯	⋯
J025257.17–010220.7	1.25	0.17	318	1871	14.16	594.8	42.0	⋯	⋯
J025316.47+010759.8	1.03	0.98	−533	−544	14.16	−215.5	−15.2	⋯	⋯
J025331.93+001624.8	1.83	0.98	655	668	14.16	−77.6	−5.5	⋯	⋯
J082012.63+431358.4	1.07	0.68	378	556	13.98	25.9	1.8	⋯	⋯
J082214.83+431701.9	0.97	0.68	−455	−669	13.98	25.9	1.8	⋯	⋯
J095656.44+535023.3	0.61	6.16	300	49	12.91	241.9	18.7	−86.2	−6.7

Note. (1) SDSS ID of the object (α_{2000} and δ_{2000}). (2) Spectroscopic redshift of the object. (3) Time baseline in Ju et al. (2013). (4) The velocity shift measured by Ju et al. (2013) with cross-correlation of rest frame wavelength window near the Mg II BEL (see section 2.2). (5) The LoS component of acceleration based on columns (3) and (4). (6) Time baseline of the SDSS IV data. (7) Velocity shift measured with cross-correlation of rest frame wavelength window near the Mg II BEL. (8) The LoS acceleration of SDSS IV follow-up Mg II measurement. (9) Velocity shift measured with SDSS IV data in the rest frame wavelength window 4761 Å $< \lambda <$ 4961 Å near the Hβ BEL (if available). (10) The LoS acceleration based on Hβ BEL measured with SDSS IV data.

$|\Delta V|$ measurements are also poor: 0.47 for $a_{\rm LoS}$, and 0.26 for ΔV. These results reveal that the detections are highly unlikely to be attributed to binary orbital motion (see Section 3.2). A comparison of $|a_{\rm LoS}|$ values is presented in Figure 2.

We consider various explanations for the large velocity offsets, which are clearly not caused by orbital motion. One possibility is merely noise spikes or imperfect sky subtraction. In Ju et al. (2013), we tried to reproduce the distribution of acceleration values using simulations of the random (e.g., photon noise) and systematic (e.g., sky subtraction) noise in the spectra. From these factors alone, we were unable to reproduce such a broad distribution. Thus, we conclude that the velocity offsets we measure are real, but are not due to binary motion. We infer that the velocity shifts should be attributed to real spectral variability, but arising from single AGN.

In the literature, velocity changes in the BLR have long been seen (e.g., Eracleous et al. 1997; Storchi-Bergmann et al. 2003; Shapovalova et al. 2004; Gezari et al. 2007; Jovanović et al. 2010; Shapovalova et al. 2010; Decarli et al. 2013; Barth et al. 2014; Popović et al. 2014; Liu et al. 2016a). In some cases these are interpreted in the context of accretion disk models (e.g., Bogdanović et al. 2008). In others, the velocity shifts can be attributed just to reverberation (Barth et al. 2014, 2015). As the continuum luminosity of the AGN varies with time, so too does the emission from photoionized gas, with a time lag. Asymmetries in the line transfer function between the continuum and line emission light curves will cause apparent velocity shifts in the BLR. Barth et al. (2015) show that these shifts can extend to at least a couple hundred km s^{-1}. Thus far, only relatively low-luminosity AGN have been monitored with high enough cadence to yield a constraint here, and in these cases the empirical velocity shifts never go higher than a few hundred km s^{-1}. We do not have a model for the the spectral variability due to reverberation or other causes (e.g., León-Tavares et al. 2013; Simić & Popović 2016), but our simulations suggest that these physical effects dominate the velocity shifts that we measure.

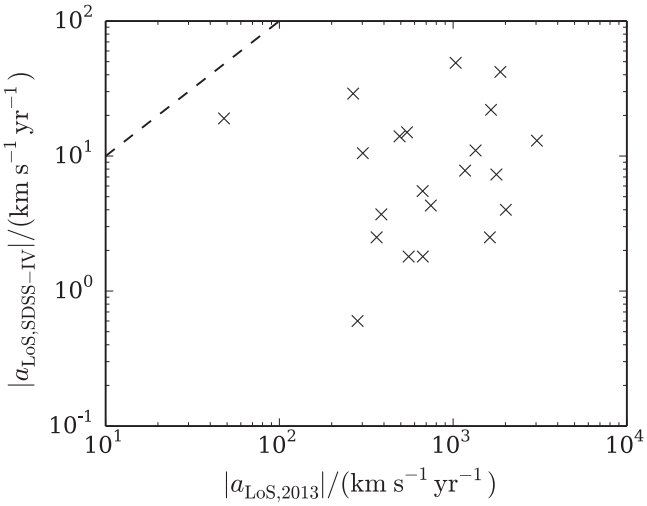

Figure 2. Comparison of the LoS acceleration measurements. Each data point indicates a row in Table 2. The horizontal axis indicates $a_{\rm LoS}$ measured in Ju et al. (2013) (median time baseline 0.98 year) , and the vertical axis indicates $a_{\rm LoS}$ obtained from the pertinent SDSS-IV data (median time baseline 8.04 year). The dashed line in the upper-left corner is the line of equal value of the two $a_{\rm LoS}$.

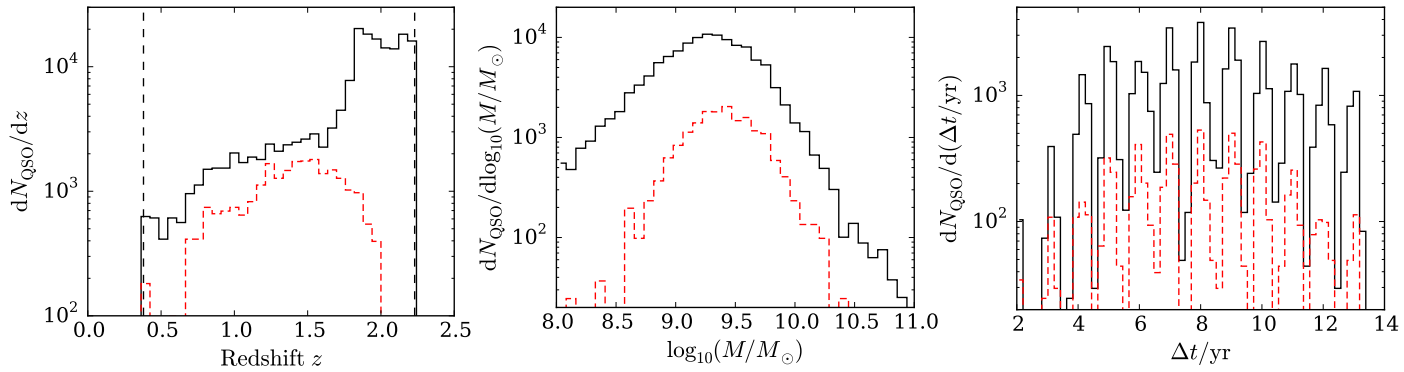

Figure 3. Basic properties of our SDSS DR7-DR12 multi-observation sample. In each panel, the black histogram shows the distribution of our whole sample, and the red dashed histogram displays that of the S/N pixel^{-1} > 3 subsample. We present the statistics only for $0.38 < z < 2.23$ objects, which have their Mg II BEL in the SDSS spectra. Left panel: redshift (z); vertical dashed lines indicate the edges of Mg II redshift window. Middle panel: logarithm of BH mass based on Shen et al. (2011) modeling of FWHM of Mg II BEL. Right panel: observed time baseline of our velocity shift detections.

3.5. Summary

From our follow-up of the Ju et al. (2013) candidates, we conclude that the broad-line variability in single AGN is a significant source of contamination in our search for binary candidates. Unfortunately, we do not yet know the full distribution of line shifts that is expected from reverberation —nor do we know whether the distribution of velocities is a function of other properties of the AGN, such as BH mass or luminosity. We are not in a position to model and remove the contribution to the measured velocity shifts from these reverberation and disk variability effects. However, velocity shifts >500 km s^{-1} have not been seen in single objects. Given the 10-year time baselines that we will present in the next section, we expect to see >1000 km s^{-1} lineshifts from orbital motion, which we do not believe can arise from single BHs. However, in the longer term, we must measure the distribution of line shifts from reverberation (e.g., using ongoing multi-object reverberation mapping campaigns; Shen & Ho 2014; Shen et al. 2015) so that we can more robustly isolate the binary candidates.

4. EXPERIMENT 2: BOSS QUASARS

4.1. Sample Properties

In addition to revisiting the Ju et al. (2013) sample (Section 3), we also build on their sample by selecting objects where the second epoch of observations was carried out by the Baryon Oscillation Spectroscopic Survey, acquiring spectroscopic redshifts of luminous red galaxies and quasars to measure cosmic large scale structure, and hence baryonic acoustic oscillations (Gunn et al. 2006; Eisenstein et al. 2011; Ross et al. 2012; Dawson et al. 2013; Smee et al. 2013). In the SDSS DR12 quasar catalog (Pâris et al. 2014; Pâris et al. 2016, in preparation), the flag "SDSS_DR7" is assigned to each object to indicate whether this object has already been observed in DR7. We specifically note that, unlike many of the objects in Ju et al. (2013), none of the objects analyzed in this paper are re-observed because of observational problems (i.e., those flagged as "bad" or "marginal").

We set the redshift range by requiring that there be at least a ±50 Å window around the Mg II λ2800 Å line in the 3800 Å < λ < 9200 Å wavelength range of the SDSS spectra, leading to a range of $0.38 < z < 2.23$. A total of 10121 quasars satisfy this redshift condition. The minimum window of ±50 Å allows us to measure velocity shifts up to ∼5353 km s^{-1}; this value is far beyond what we actually detect, as we will see in Section 4.2.

In Figure 3, we present some basic properties of the BOSS multi-epoch sample and the high-S/N subsample (S/N pixel^{-1} > 3). The value of S/N pixel^{-1} is defined in a different way here as compared to Ju et al. (2013). In this work, we evaluate the S/N in the rest-frame wavelength window surrounding the Mg II BEL (2698 Å < λ < 2798 Å typically, but at least 2748 Å < λ < 2848 Å) *after* subtracting the continuum (see Section 2.1 for continuum subtraction). There are 1438 high-S/N objects, out of the 10121 QSOs that fall in the redshift window.

We span a range of observed time baselines from 1.91 to 13.34 year with a median of 8 year, considerably longer than the mean time difference of 0.7 year observed by Ju et al. (2013). The absolute magnitude in the *i*-band (Fukugita et al. 1996) ranges from −21.11 through −29.79 mag with median −26.56 mag. Using standard scalings between broad-line width, AGN luminosity, and BH mass (Shen et al. 2011), we find a median BH mass of $1.8 \times 10^9\,M_\odot$, with a standard deviation of 1.24 dex in log BH mass. Because of ambiguity in the BLR dynamics in binary systems, we will adopt a range of BH mass values (see Section 5). The median redshift is $\langle z \rangle = 1.92$, with standard deviation 0.39 (Figure 3).

4.2. Results

In the SDSS DR12 sample of quasars with multiple observations, we focus on the 1438 objects with S/N pixel^{-1} > 3 (Section 3.1) to investigate ΔV. The distribution function of ΔV, for both the whole sample and the S/N pixel^{-1} > 3 subsample, is presented in Figure 4. The distribution function of the entire sample is centered at −2.6 km s^{-1} with $\sigma \simeq 220$ km s^{-1}. For the S/N pixel^{-1} > 3 subsample, the distribution function is centered at 9.8 km s^{-1}, with $\sigma \simeq 90$ km s^{-1}. For completeness, we manually inspect those objects with intermediate S/N pixel^{-1} > 1 and large $|\Delta V| > 1000$ km s^{-1}. None of those "high-ΔV outliers" are trustworthy: the high values result from highly discrepant pixels or variable absorption features. Therefore, in what follows, we focus on the S/N pixel^{-1} > 3 sample.

We follow Ju et al. (2013) and tabulate all targets with $|\Delta V| > 3\sigma \simeq 270$ km s^{-1} (that is, more than 3σ outliers from the full distribution) in Table 3. We have removed 16 out of 33 objects where the apparent large velocity was caused by highly

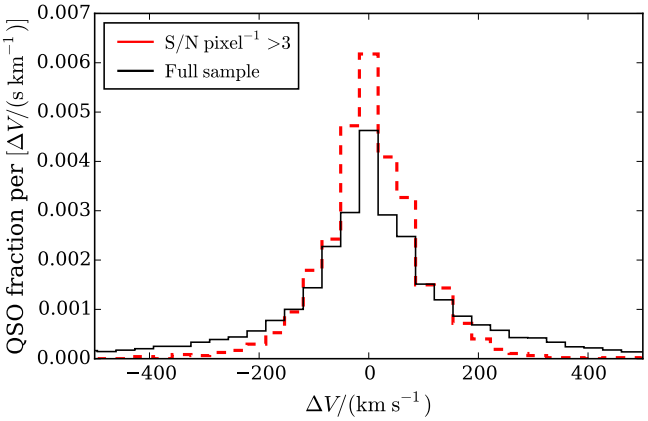

Figure 4. Distribution function of ΔV, measured by cross-correlating the Mg II BEL of the two epochs of observation, the latter coming from the SDSS DR12. The thin black histogram represents the distribution function of the whole sample, whereas the thick red dashed histogram is for the S/N pixel$^{-1} > 3$ subsample.

discrepant pixels or broad and variable absorption features, leaving 14 in the table. There are very few objects that fall above our nominal $|\Delta V|$ limit. Furthermore, we have already shown in Section 3.4 (above) that most of the velocity shifts of order $\sim$300 km s^{-1} are not due to orbital motion. However, we tabulate these quasars for completeness and to demonstrate the small total number of them. In addition, one (and the only) object in Table 3 with $|\Delta V| > 5\sigma = 450$ km s^{-1} is presented in the bottom row of Figure 1.

The percentage of objects showing outlying values of $|\Delta V|$ is quite small. However, given that we are probing typical timescales of a decade, we would expect to encounter some significant velocity shifts from a population of sub-parsec binary BHs among typical QSOs. In the next section, we use gas-assisted inspiral models from Rafikov (2013, 2016) to quantify this expectation.

5. MODELING AND INTERPRETATION

To interpret our findings in terms of the SMBH binary occurrence rates, we need to know the fraction of time that a binary with a given set of characteristics (mass, mass ratio, etc.) spends at a particular orbital separation through its lifetime. That requires knowledge of the residence time $|d\ \ln a/dt|^{-1}$, which can be computed once the processes driving binary inspiral are specified.

Following Ju et al. (2013), we will focus on the sub-parsec orbital evolution of the binary driven by its gravitational coupling with the surrounding circumbinary disk, which must exist around the binary to fuel its quasar activity. Tidal interaction of the binary with the disk (Goldreich & Tremaine 1980; Artymowicz & Lubow 1994) results in angular momentum exchange between the two, leading to binary inspiral. The angular momentum of the sub-parsec binary is absorbed by the gas in the inner regions of these accretion disks, and is then transported outwards by viscous stresses (Rafikov 2013, 2016).

In this work, we follow the description of the disk-binary coupling in Rafikov (2013), which should be consulted for details. In these models, one self-consistently follows the coupled viscous evolution of the disk and the orbital inspiral of the binary. In particular, the non-local nature of the viscous coupling (i.e., the time evolution of the "radius of influence," out to which internal stresses propagate binary perturbation at a given moment of time) is fully accounted for, compared to other (quasi-) steady-state models (e.g., Haiman et al. 2009) or purely self-similar solutions (e.g., Ivanov et al. 1999). The behavior of the internal stress in our circumbinary disk models is characterized by the dimensionless viscosity parameter $\alpha = 0.1$.

One of the key characteristics that determines both the SMBH inspiral and the disk evolution in the models of Rafikov (2013) is the gas accretion rate through the disk far outside the binary orbit $\dot{M}_\infty$. We often quantify this rate via the Eddington ratio $\dot{m}_{\rm Edd} \equiv \dot{M}_\infty/\dot{M}_{\rm Edd}$, which is a free parameter in our calculations. The value of $\dot{M}_{\rm Edd}$ is determined for the mass of the secondary[6], which is assumed to be the main accretor (see below). The disk-binary evolution models of Rafikov (2013) assume that a binary accretes only a small fraction (e.g., below several tens of per cent) of the incoming gas, in agreement with MacFadyen & Milosavljević (2008). Most of the mass accumulates in the inner disk, increasing the rate of the angular momentum exchange between the disk and the binary. As demonstrated by Rafikov (2016), this assumption results in the highest possible torque on the binary for a given $\dot{M}_\infty$, meaning the *fastest* orbital inspiral. We will comment on the implications of this assumption in Section 6.

Another important parameter of the model is the binary mass ratio $q \equiv M_{\rm s}/M_{\rm p}$—the ratio of the secondary to primary BH mass. It is generally thought that the secondary BH should intercept most of the accretion flow from the circumbinary disk (e.g., Cuadra et al. 2009; Roedig et al. 2011, 2012; Farris et al. 2014; Roedig & Sesana 2014). If the secondary BH is luminous enough to be seen as a quasar at $z \approx 1$ (i.e., be included in our sample), then the mass ratio must be close to unity, because the observed luminosities already require secondary BH masses $>10^8\,M_\odot$. For that reason, in this work, we explore the values of q ranging from 10^{-2} to 1.

The binary typically starts at large separation in the so-called "disk dominated regime," when the "local disk mass" $M_d \equiv \Sigma r^2$ (Σ is the disk surface density) exceeds the mass of the secondary $M_{\rm s}$. Then, the binary inspiral is believed to be governed by the viscous timescale of the disk, making the residence timescale largely independent of the secondary mass: $|d\ \ln a/dt|^{-1} \sim t_\nu \equiv r^2/\nu$. However, later on, as the binary orbit shrinks, the local disk mass becomes lower than M_s, according to our calculations that fully account for the back-reaction of the binary torque on the circumbinary disk structure. This effect ultimately makes the residence time sensitive to the mass of the secondary.

Our calculations assume that binary orbits are circular. There are simulations showing that high eccentricity may arise through binary-star interactions (e.g., Sesana et al. 2008; Sesana 2010; Preto et al. 2011; Khan et al. 2012; Sesana & Khan 2015; Vasiliev et al. 2015) and binary-disk interactions (e.g., Armitage & Natarajan 2005; Cuadra et al. 2009; Roedig et al. 2011; Roedig & Sesana 2014). However, given the lack of observational evidence regarding this issue, we opted for the simplest possible assumption of circular orbits.

We start the binary at 0.1 pc, which is a typical stalling radius for the inspiral driven by purely stellar dynamical processes (Yu 2002). We also consider models with 0.3 pc initial separation, which are used for comparison. The binary

[6] We adopt radiative efficiency $\epsilon = 0.1$ as is commonly assumed for the AGN accretion disks.

Table 3
High-ΔV and High-SNR Subsample Based on BOSS Data

SDSS ID	z	$\log_{10}M_{\rm BH}$ ($M_\odot$)	Δt (year)	ΔV (km s^{-1})	$a_{\rm LoS}$ (km s^{-1} yr^{-1})
(1)	(2)	(3)	(4)	(5)	(6)
J002127.88+010420.2	1.82	9.81	9.81	−345	−35
J003333.61–001858.1	0.69	9.27	10.03	293	29
J014822.62+132142.6	0.88	9.36	10.33	−345	−33
J091344.40+150935.1	0.94	9.45	5.28	−276	−52
J095929.88+633359.8	1.85	10.74	11.14	−328	−29
J103623.66+152733.3	1.92	9.95	5.02	328	65
J105611.27+170827.5	1.33	9.62	5.93	−293	−49
J110038.79+282036.1	1.79	9.60	7.06	258	36
J125238.51+115557.1	1.85	9.64	6.87	310	45
J133615.79+495529.0	1.50	9.62	8.13	−207	−25
J135109.38+320049.0	1.12	9.64	4.85	−328	−67
J135218.49+224708.9	1.45	10.09	4.24	−397	−93
J163600.37+432802.7	0.94	9.42	11.00	276	25
J163709.31+414030.8	0.76	9.76	10.99	448	40

Note. (1) SDSS ID of the object. (2) Spectroscopic redshift of the object. (3) Logarithm of mass of the SMBH in solar masses, using the results in Shen et al. (2011), the FWHM of Mg II BEL (model S10). (4) Time baseline of our velocity shift measurement. (5) Velocity shift measured with BEL specified in column (3). (6) LoS acceleration. Spectra and correlation functions of objects in this table, which have prominent $|\Delta V|$, are shown as examples in Figure 1; they are: J014822.62 +132142.6, J125238.51+115557.1, and J163709.31+414030.8.

BH orbit is evolved until its semimajor axis becomes equal to the radius of BLR (e.g., Shen & Loeb 2010),

$$R_{\rm BLR} = 2.2 \times 10^{-2}\,{\rm pc} \times \left(\frac{L_{\rm bol}}{1.26 \times 10^{45}\,{\rm erg\ s^{-1}}}\right)^{3/2}. \quad (7)$$

At this point, we assume that the BLR around the secondary is destroyed and we may no longer expect to detect periodic shifts of the BELs due to the orbital motion of the secondary. This radius represents a large uncertainty in our method.

Using these assumptions, we calculate the residence time as a function of radius as the binary evolves under the influence of tidal coupling to the disk. An example of the calculated residence times is shown in Figure 5, as adapted from Ju et al. (2013). The figure shows the fiducial case, where the Eddington ratio $\dot{m}_{\rm Edd} = 0.1$, and mass ratio $q = 1$. As the accretion rate $\dot{m}_{\rm Edd}$ increases, or the mass ratio q decreases, disk torques become more important to the motion of secondary, hence shortening the residence time. In practice, grid data of separation $\{r_i\}$ and the corresponding evolution time $\{t_i\}$ are generated, which will be utilized in the following discussions.

We use the predicted residence times as a function of orbital separation to calculate (a) what fraction of objects would be observable with velocity shifts greater than 450 km s^{-1}, as a function of the total time baseline and (b) the full expected distribution of velocity offsets. These fractions assume that *all* the QSOs are binaries. To perform this calculation, we adopt a range of BH masses based on luminosity (and assuming a range of accretion rates, described below), and $\Delta\tau \equiv \Delta t/(1+z)$ (the time lapse in the object rest frame) between the most widely separated epochs. Once again, we always assume that only the secondary BH carries a BLR.

With these assumptions, we obtain an interpolated grid of data, giving the relation, on the ith grid point, between the separation of the binary r_i and the time t_i that the binary takes to evolve from $r = 0.1$ pc to this r_i. On each grid point, we calculate the expected value of $|\Delta V|$, after marginalizing over

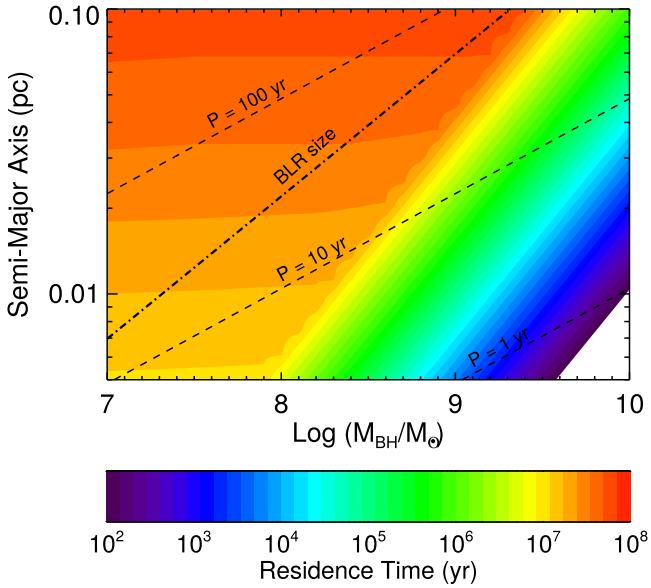

Figure 5. SMBH binary residence time $t_{\rm res}$, as a function of radius r and the total mass of the binary system $M_{\rm BH}$. Here we only show the "fiducial" example (see others in Ju et al. 2013), which has Eddington ratio $\dot{m}_{\rm Edd} = 0.1$ and SMBH mass ratio $q = 1$. The dashed lines are the overlaid contours of constant orbital period. The dashed–dotted line indicates the size of the BLR.

orbital phase ($0 < \phi < 2\pi$) and the cosine of inclination angle. To be general, we consider that we could preferentially miss nearly edge-on systems due to obscuration (Antonucci & Miller 1985). We parametrize the opening angle of the obscuration with a critical angle i_c, such that objects with $i_c < i < (\pi - i_c)$ are likely to be obscured. We consider two cases, one with no obscuration, $i_c = \pi/2$, and the other with $i_c = \pi/3$ (e.g., Hasinger 2008)

$$\langle|\Delta V|\rangle_i = V_{\rm co}(r_i)\langle|\cos(\phi + \Omega\Delta\tau) - \cos\phi|\rangle_\phi \langle|\sin i|\rangle_{\cos i}$$
$$= V_{\rm co}(r_i)\sin\left(\frac{\Omega\Delta\tau}{2}\right) \times \left[\frac{2i_c - \sin(2i_c)}{\pi(1-\cos i_c)}\right], \quad (8)$$

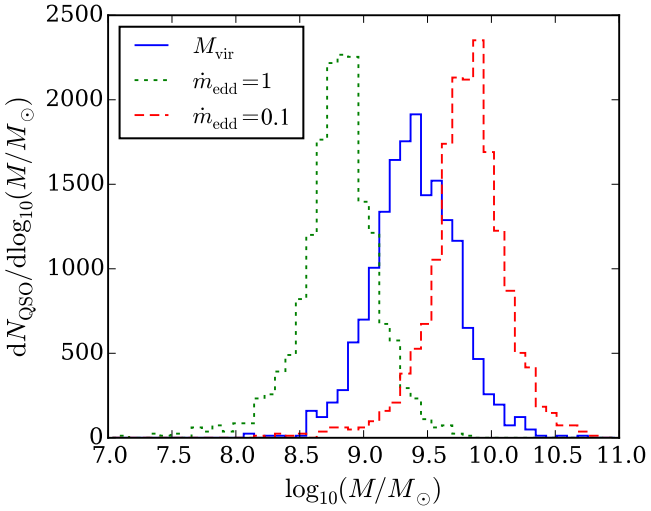

Figure 6. Secondary SMBH mass estimated by different methods, using Mg II line width (blue histogram Shen et al. 2011), and bolometric luminosity assuming $\dot{m}_{\rm Edd}=0.1$ (red dashed histogram) or $\dot{m}_{\rm Edd}=1$ (green dotted histogram).

where Ω is the angular velocity of orbital motion specified by Equation (5) at radius r_i, $V_{\rm co}(r_i)$ is the magnitude of the orbital linear velocity at r_i relative to the center of mass, and $M_{\rm BH}$ is again the mass of the secondary instead of the total,

$$V_{\rm co}(r_i)\equiv\left[\frac{GM_{\rm BH}}{rq\,(1+q)}\right]^{1/2}. \quad (9)$$

It is straightforward to prove that Equation (8) reduces to $\langle|\Delta V|\rangle_i = V_{\rm co}(r_i)\sin(\Omega\Delta\tau/2)$ at $i_c=\pi/2$, our fiducial case.

For every r_i, a value of $\langle|\Delta V|\rangle$ is evaluated, which is weighted with $(\delta\tau)_i\equiv(\tau_{i+1}-\tau_{i-1})$ to generate a histogram. This histogram is, by definition, the probability distribution function of $|\Delta V|$ of this quasar. Stacking the distribution functions of every quasar in our sub-sample, we obtain the expected distribution function of $|\Delta V|$ of the whole ensemble. The mass ratio q, accretion rate $\dot{m}_{\rm Edd}$ relative to the Eddington limit, and BLR size $R_{\rm BLR}$ of these quasars are quite uncertain. To bracket the resulting uncertainties, we assume different q (1 and 0.1), $\dot{m}_{\rm Edd}$ (0.1 and 1), and $R_{\rm BLR}$ (0.5–2 times the size in Equation (7)), to explore a plausible region in parameter space.

To make our calculations self-consistent, we adopt a single luminosity for the BH as measured, and then assume that the BH is radiating at either 10 or 100% of the Eddington luminosity to derive the BH mass. These two assumptions bracket the virial estimate based on Mg II from Shen et al. (2011), as shown in Figure 6.

Figure 7 presents the two statistics (observable fraction and $|\Delta V|$). In the left panel, the upper limit on our observational fraction is represented by the black star. The right panel shows the expected distributions in velocity, again assuming that the target binary starts evolving at $r=0.1$ pc. The expected velocity distributions range from 500 to 10^4 km s^{-1}. As we discuss in Section 6, given the typical lifetimes of quasars and our estimated residence times, we would naively expect to detect a few large velocity shifts. That we find no velocity shifts of this magnitude places a real constraint on the length of time that binary BHs spend at sub-parsec separations in an active phase, even given substantial uncertainties on the BLR size.

6. DISCUSSION AND SUMMARY

This paper presents two exercises aimed at constraining the statistics of binary SMBHs with sub-parsec separation. First, we present follow-up of the binary SMBH candidates first presented in Ju et al. (2013), using new observations of 21 of the quasars that were observed to display radial velocity shifts >270 km s^{-1} in that paper. Here, we examine whether the observed radial velocity shifts grow larger with longer time baselines, as would typically be expected if they were due to orbital motion. Cross-correlation of the Mg II BEL region over roughly a decade shows considerably lower empirical LoS acceleration ($a_{\rm LoS}$) in each object as compared to the previous detections, and is inconsistent with orbital motion.

Second, we extend the methodology of Ju et al. (2013) and examine repeat observations of these quasars in the SDSS/BOSS data. Among them, 1438 have a Mg II BEL detected with S/N pixel^{-1} > 3. The velocity shift distribution function, measured through cross-correlation, peaks at ∼9 km s^{-1} and has $\sigma\sim 90$ km s^{-1} as its dispersion. The high S/N subsample yields 15 objects with $|\Delta V|>3\sigma\simeq 270$ km s^{-1}, whereas there is only one object in the $|\Delta V|>5\sigma\simeq 450$ km s^{-1} regime. Because we have demonstrated that velocity shifts of ∼300 km s^{-1} can occur in quasars without binaries, we prefer to adopt the more conservative value of 450 km s^{-1} as a possible indicator of orbital motion in a binary. Comparing this single candidate with theoretical expectations, we conservatively find that $\lesssim$1.6% of SMBH reside in sub-parsec binaries.[7]

Our simulations suggest that quasars spend at least a Myr to reach radii where gravitational radiation can bring coalescence. Given fiducial quasar lifetime estimates of 10^7–10^8 year (Martini & Weinberg 2001), we should have detected a few binaries in our sample. This inferred ratio is quite sensitive to the uncertainties in the BH mass measurements and BLR sizes. Nevertheless, given our relatively long time baselines and large numbers of objects, we should be detecting large velocity shifts if merging BH binaries spend the amount of time expected from simulations in a sub-parsec quasar phase.

Assuming fiducial values for the BH binary of $\dot{m}_{\rm Edd}=0.1$ and $r_0=0.1$ pc, and a BLR size in accordance with Shen & Loeb (2010), we find that $\lesssim$1% of the quasar population is in a sub-parsec phase. These are the only observational limits on the residence times of BH binaries with ∼0.1 pc separations at cosmological distances, and (if taken at face value) they suggest that BH binaries spend a surprisingly short period of time in this phase compared to our models.

There are some major caveats. As is shown in Figure 7, the upper limit on the sub-parsec binary fraction is extremely sensitive to BLR size, from 0.1% with a BLR size one half as large, to ∼100% with a doubled BLR size. If the starting point is set to be as large as 0.3 pc, our limit on the observable fraction drops to $\lesssim$0.2%.

On the other hand, in our gas-assisted binary inspiral scenario, the binary occurrence rate should be independent of the accretion history of the binary. Indeed, we observe the binary as an AGN only while it is actively accreting, and this is also the period when its orbit is evolving due to disk torques. As long as the mass supply switches off and the gas-driven binary inspiral stalls (assuming that the gravitational wave

[7] We also tested increasing the sample by adopting a lower SNR limit (S/N pixel^{-1} > 1). We derive a similar limit on the sub-parsec fraction with that alternate sample.

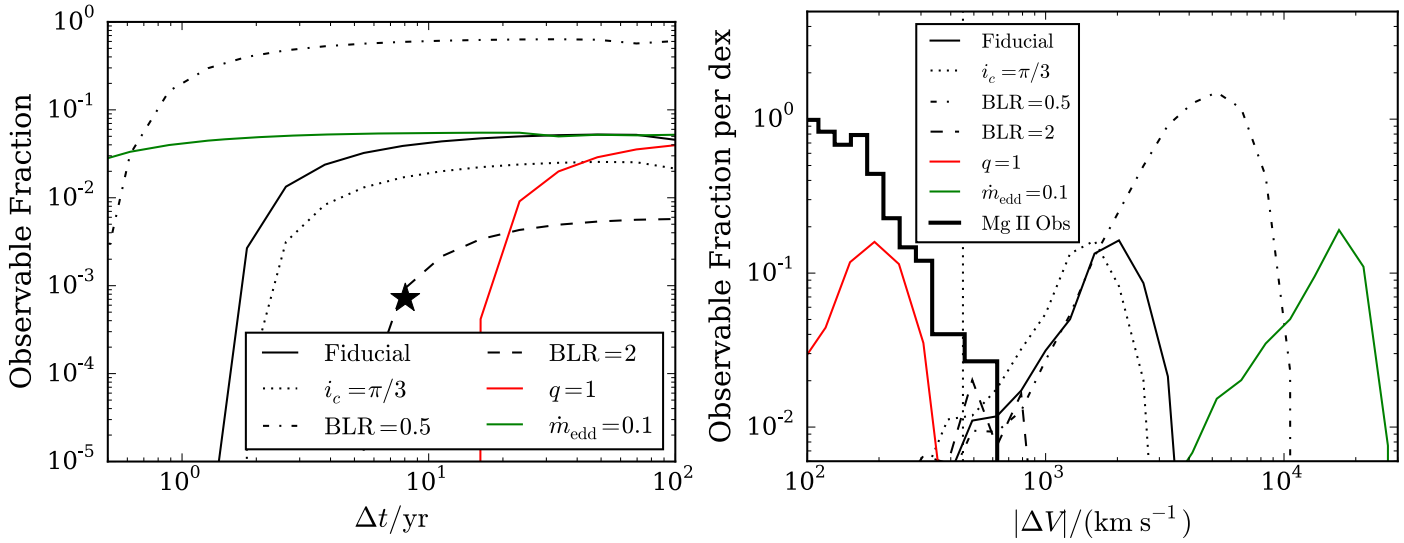

Figure 7. Observability of binary SMBHs, comparing theoretical predictions and observation data. Our observation results are from the S/N pixel^{-1} > 3 sub-sample using the SDSS DR12 observation data, measuring the Mg II BEL cross-correlation velocity shift. Left panel: fraction of SMBHs that have greater velocity shift than the 5σ (450 km s^{-1}) threshold. Observation result is indicated by the star symbol. The "fiducial" light black solid curve has $q = 0.1$, $\dot{m}_{\rm Edd} = 1$, "standard" BLR size (Equation (7)), and $i_c = \pi/2$. Other curves have one parameter different from the fiducial one, which is indicated in the legend. Right panel: the distribution functions of $\log_{10}|\Delta V|$. The thick black histogram on the left shows observation results. Theoretical curves have the same denotations with color and line style as in the central panel. A vertical dashed line shows the $|\Delta V| = 5\sigma \simeq 450$ km s^{-1} threshold.

emission is not yet capable of shrinking the orbit efficiently), we simply stop observing such systems, which thus naturally removes them from our sample of observed objects and does not affect the statistics of luminous AGNs.

It should also be kept in mind that our model assumptions tend to *minimize* the estimated BH binary residence time for a given separation. As mentioned in Section 5, our assumption of significantly suppressed accretion onto the binary (compared to $\dot{M}_\infty$) results in the highest value of the angular momentum loss experienced by the binary (for a given $\dot{M}_\infty$), meaning that it spends the shortest time per interval of the semimajor axis. Allowing the binary to accrete from the disk more readily, in agreement with some recent simulations (Farris et al. 2014; Shi & Krolik 2015), would reduce mass accumulation in the inner disk and *lower* the torque on the binary, as demonstrated in Rafikov (2013, 2016). As a result, the binary would spend *more time* in the separation range probed by the cadence of our sample, exacerbating the conflict with our non-detection of significant line shifts. Thus, our model assumptions effectively imply that the inferred constraint on the SMBH binary occurrence rate is in fact an *upper limit*. In that sense, our conclusion that this phase of binary evolution should be shorter than expected is robust.

First, we address the origin of the $\sim$300 km s^{-1} velocity shifts that we observe in a small sub-sample of objects. The Ju et al. (2013) sample displays large velocity shifts that cannot be ascribed to orbital motion. We have asserted that the $\sim$300 km s^{-1} velocity shifts are not due to noise. Here, we address the origin. Other possible sources must be considered to explain the velocity shift. One possibility is recoiling SMBHs. These might well present similar effects in terms of velocity offset, but with temporal changes that are not sustained in a way similar to binary systems (e.g., Bekenstein 1973; Fitchett & Detweiler 1984; Blanchet et al. 2005; Civano et al. 2010, 2012; Blecha et al. 2013).

We can also compare our conclusions with results from other techniques to find the electromagnetic signatures of tight binaries. These techniques often probe shorter orbital periods, but also point toward short residence times. In particular, using quasi-periodic photometric variability, Graham et al. (2015b) present 111 candidate binaries out of a sample of 243,500 quasars mostly with $z \sim 1$–2 but extending to $z = 4$. Similarly, Charisi et al. (2016) find 33 candidates out of 35,383 quasars with a median redshift $z \sim 2$, and Liu et al. (2016b) identify <1 candidates out of 670 quasars. Given their orbital periods of 0.3–6 year, these candidates have orbital separations a factor of 7–40 smaller than ours, orbital separations that we are not sensitive to with our method. Also, at these radii, the inspiral may be dominated by gravitational radiation. According to Graham et al. (2015b), their detected fraction of 10^{-4} is a factor of $\sim$5 lower than expected based on simulations (Volonteri et al. 2009).

Our finding (assuming that $\dot{m}_{\rm Edd} = 0.1$ and $r_0 = 0.1$ pc, and a BLR size in accordance with Shen & Loeb 2010) that $\lesssim$1% of the quasar population is in a sub-parsec phase is consistent with other existing observational limits. When we adopt an initial radius of $r_0 = 0.3$ pc, the population fraction drops to 0.3%.

At lower redshifts, based on double-peaked BELs, Boroson & Lauer (2009) find that only 10^{-4}–10^{-3} quasars are in a sub-parsec phase (similar to our raw limit of a few $\times 10^{-3}$). Nominally, these results are also consistent with the sub-parsec binary fractions found by Volonteri et al. (2009), at comparable redshifts of $z \lesssim 0.7$. In the context of their merger-driven quasar model, they report that the observable fraction of binary BHs would increase by a factor of 5–10 if they examined $0.7 < z < 1$. Simulations tuned to our redshift window are needed to determine the expected sub-parsec binary fraction, given quasars triggered by merging and gas-assisted merging timescales (e.g., Kelley et al. 2016).

The Pulsar Timing Arrays (PTAs) are also gaining the required sensitivity to rule out regions of parameter space for tight SMBH binaries (e.g., Taylor et al. 2016; The NANOGrav Collaboration 2016). Pulsar timing is sensitive to the stochastic superposition of weak gravitational waves from SMBH binaries at sub-parsec scales, at which SMBH binaries are supposed to spend some of their life time. Shannon et al. (2015) were able to rule out the most optimistic theoretically predicted numbers of sub-parsec BH binaries (based on contemporary star-assisted or gas-assisted dissipation models, e.g., Wyithe & Loeb 2003, Kulier et al. 2015, and especially Ravi et al. 2015), using existing PTA constraints on the stochastic GWB. It is interesting that our constraints and those from the PTAs point in a similar direction toward short residence times at small separations.

The low frequency of the BH binary systems, particularly the lack of detection of high-velocity line shifts, start to place an interesting limit on the binary SMBH evolution picture. Although our current interpretation of the observations uses a particular model of binary inspiral, we still believe that it provides an interesting constraint.

If all quasars are triggered by merging, and the AGN lifetime is only $\sim 10^8$ year, then our results indicate that quasars spend a much lower fraction of their lifetimes in a sub-parsec phase than our relatively conservative gas-assisted theories predict. Given the limitations of our method, we are left with a few possible interpretations of our findings. One is that the binary BH (or at least the secondary) does not radiate efficiently in this phase. Second, the BLR may be much larger than we believe, encompassing the whole binary, such that the signs of the orbital motion cannot be observed. Third, all BH binaries may stall at radii larger than $\gtrsim 0.3$ pc, outside of our range of interest. Fourth, the most interesting possibility is that BH binaries merge much more rapidly than our models predict.

Extensions of our work would involve detections of velocity shifts using more BELs. For example, the C IV λ1549 Å BEL is often more luminous than Mg II adopted in this paper. Nevertheless, the C IV BEL is generally expected to emerge from the inner region of the BLR. Its characteristics are more vulnerable to complicated quasar physics, especially outflows, which are not fully understood at this moment (e.g., Proga et al. 2000; Proga & Kallman 2004; Proga 2005, 2007; Higginbottom et al. 2014), showing absorption and asymmetry that may introduce an extra bias into velocity shift detection. Going forward, we must pursue as many independent electromagnetic constraints on the sub-parsec binary BH population as possible, as we prepare for the the first PTA detections. Our observational results also strongly motivate further theoretical work to better understand the orbital evolution of the SMBH binaries.

Roman R. Rafikov is an IBM Einstein Fellow at the Institute of Advanced Study; his financial support is provided by the NSF via grants AST-1409524, AST-1515763, NASA via grants 14-ATP14-0059, 15-XRP15-2-0139, and The Ambrose Monell Foundation. Jenny E. Greene acknowledges funding from the National Science Foundation under Grant No. AAG: #1310405. We are thankful to Dr. Adam Myers, Dr. Michael Eracleous, and Dr. Zoltan Haiman for useful comments and suggestions.

REFERENCES

Abadie, J., Abbott, B. P., Abbott, R., et al. 2011, PhRvD, 83, 122005
Amaro-Seoane, P., Aoudia, S., Babak, S., et al. 2013, GWN, 6, 4
Antonucci, R. R. J., & Miller, J. S. 1985, ApJ, 297, 621
Armitage, P. J., & Natarajan, P. 2005, ApJ, 634, 921
Artymowicz, P., & Lubow, S. H. 1994, ApJ, 421, 651
Barausse, E., & Rezzolla, L. 2009, ApJL, 704, L40
Barnes, J. E., & Hernquist, L. 1992, ARA&A, 30, 705
Barth, A. J., Bennert, V. N., Canalizo, G., et al. 2015, ApJS, 217, 26
Barth, A. J., Voevodkin, A., Carson, D. J., & Woźniak, P. 2014, AJ, 147, 12
Begelman, M. C., Blandford, R. D., & Rees, M. J. 1980, Natur, 287, 307
Bekenstein, J. D. 1973, ApJ, 183, 657
Blanchet, L., Qusailah, M. S. S., & Will, C. M. 2005, ApJ, 635, 508
Blecha, L., Civano, F., Elvis, M., & Loeb, A. 2013, MNRAS, 428, 1341
Bogdanović, T., Smith, B. D., Sigurdsson, S., & Eracleous, M. 2008, ApJS, 174, 455
Boroson, T. A., & Lauer, T. R. 2009, Natur, 458, 53
Burke-Spolaor, S. 2011, MNRAS, 410, 2113
Charisi, M., Bartos, I., Haiman, Z., et al. 2016, arXiv:1604.01020
Charisi, M., Bartos, I., Haiman, Z., Price-Whelan, A. M., & Márka, S. 2015, MNRAS, 454, L21
Civano, F., Elvis, M., Lanzuisi, G., et al. 2010, ApJ, 717, 209
Civano, F., Elvis, M., Lanzuisi, G., et al. 2012, ApJ, 752, 49
Cuadra, J., Armitage, P. J., Alexander, R. D., & Begelman, M. C. 2009, MNRAS, 393, 1423
Dawson, K. S., Kneib, J.-P., Percival, W. J., et al. 2015, arXiv:1508.04473
Dawson, K. S., Schlegel, D. J., Ahn, C. P., et al. 2013, AJ, 145, 10
Decarli, R., Dotti, M., Fumagalli, M., et al. 2013, MNRAS, 433, 1492
Decarli, R., Dotti, M., Montuori, C., Liimets, T., & Ederoclite, A. 2010, ApJL, 720, L93
Eisenstein, D. J., Weinberg, D. H., Agol, E., et al. 2011, AJ, 142, 72
Eracleous, M., Boroson, T. A., Halpern, J. P., & Liu, J. 2012, ApJS, 201, 23
Eracleous, M., Halpern, J. P., Gilbert, A. M., Newman, J. A., & Filippenko, A. V. 1997, ApJ, 490, 216
Farris, B. D., Duffell, P., MacFadyen, A. I., & Haiman, Z. 2014, ApJ, 783, 134
Fitchett, M. J., & Detweiler, S. 1984, MNRAS, 211, 933
Fukugita, M., Ichikawa, T., Gunn, J. E., et al. 1996, AJ, 111, 1748
Gaskell, C. M. 1983, in Liege International Astrophysical Colloquia, Vol. 24, Quasars and Gravitational Lenses, ed. J. P. Swings (Liege: Univ. de Liege), 473
Gergely, L. Á., & Biermann, P. L. 2012, arXiv:1208.5251
Gezari, S., Halpern, J. P., & Eracleous, M. 2007, ApJS, 169, 167
Gezari, S. T. K. 2005, PhD thesis, Columbia Univ.
Gibson, R. R., Brandt, W. N., Gallagher, S. C., Hewett, P. C., & Schneider, D. P. 2010, ApJ, 713, 220
Gibson, R. R., Brandt, W. N., Schneider, D. P., & Gallagher, S. C. 2008, ApJ, 675, 985
Gold, R., Paschalidis, V., Ruiz, M., et al. 2014, PhRvD, 90, 104030
Goldreich, P., & Tremaine, S. 1980, ApJ, 241, 425
Graham, M. J., Djorgovski, S. G., Stern, D., et al. 2015a, Natur, 518, 74
Graham, M. J., Djorgovski, S. G., Stern, D., et al. 2015b, MNRAS, 453, 1562
Gunn, J. E., Siegmund, W. A., Mannery, E. J., et al. 2006, AJ, 131, 2332
Haiman, Z., Kocsis, B., & Menou, K. 2009, ApJ, 700, 1952
Hasinger, G. 2008, A&A, 490, 905
Higginbottom, N., Proga, D., Knigge, C., et al. 2014, ApJ, 789, 19
Hofmann, F., Barausse, E., & Rezzolla, L. 2016, ApJL, 825, L19
Ivanov, P. B., Papaloizou, J. C. B., Paardekooper, S.-J., & Polnarev, A. G. 2015, A&A, 576, A29
Ivanov, P. B., Papaloizou, J. C. B., & Polnarev, A. G. 1999, MNRAS, 307, 79
Jovanović, P., Popović, L. Č., Stalevski, M., & Shapovalova, A. I. 2010, ApJ, 718, 168
Ju, W., Greene, J. E., Rafikov, R. R., Bickerton, S. J., & Badenes, C. 2013, ApJ, 777, 44
Kelley, L. Z., Blecha, L., & Hernquist, L. 2016, MNRAS, arXiv:1606.01900
Khan, F. M., Fiacconi, D., Mayer, L., Berczik, P., & Just, A. 2016, arXiv:1604.00015
Khan, F. M., Preto, M., Berczik, P., et al. 2012, ApJ, 749, 147
Kormendy, J., & Ho, L. C. 2013, ARA&A, 51, 511
Kulier, A., Ostriker, J. P., Natarajan, P., Lackner, C. N., & Cen, R. 2015, ApJ, 799, 178
León-Tavares, J., Chavushyan, V., Patiño-Álvarez, V., et al. 2013, ApJL, 763, L36
Liu, J., Eracleous, M., & Halpern, J. P. 2016a, ApJ, 817, 42
Liu, T., Gezari, S., Burgett, W., et al. 2016b, arXiv:1609.09503
Lundgren, B. F., Wilhite, B. C., Brunner, R. J., et al. 2007, ApJ, 656, 73

MacFadyen, A. I., & Milosavljević, M. 2008, ApJ, 672, 83
Martini, P., & Weinberg, D. H. 2001, ApJ, 547, 12
Merritt, D., & Milosavljević, M. 2005, LRR, 8, 8
Morganson, E., Green, P. J., Anderson, S. F., et al. 2015, ApJ, 806, 244
Myers, A. D., Palanque-Delabrouille, N., Prakash, A., et al. 2015, ApJS, 221, 27
Nguyen, K., & Bogdanović, T. 2016, ApJ, 828, 68
Pâris, I., Petitjean, P., Aubourg, É., et al. 2014, A&A, 563, A54
Pâris, I., Petitjean, P., Ross, N. P., et al. 2016, arXiv:1608.06483
Phinney, E. S. 2001, arXiv:astro-ph/0108028
Popović, L. Č., Shapovalova, A. I., Ilić, D., et al. 2014, A&A, 572, A66
Preto, M., Berentzen, I., Berczik, P., & Spurzem, R. 2011, ApJL, 732, L26
Proga, D. 2005, ApJL, 630, L9
Proga, D. 2007, ApJ, 661, 693
Proga, D., & Kallman, T. R. 2004, ApJ, 616, 688
Proga, D., Stone, J. M., & Kallman, T. R. 2000, ApJ, 543, 686
Quinlan, G. D. 1996, NewA, 1, 35
Rafikov, R. R. 2013, ApJ, 774, 144
Rafikov, R. R. 2016, ApJ, 827, 111
Ravi, V., Wyithe, J. S. B., Shannon, R. M., & Hobbs, G. 2015, MNRAS, 447, 2772
Rodriguez, C., Taylor, G. B., Zavala, R. T., et al. 2006, ApJ, 646, 49
Roedig, C., Dotti, M., Sesana, A., Cuadra, J., & Colpi, M. 2011, MNRAS, 415, 3033
Roedig, C., & Sesana, A. 2014, MNRAS, 439, 3476
Roedig, C., Sesana, A., Dotti, M., et al. 2012, A&A, 545, A127
Ross, N. P., Myers, A. D., Sheldon, E. S., et al. 2012, ApJS, 199, 3
Ruan, J. J., Anderson, S. F., Green, P. J., et al. 2016, arXiv:1602.02752
Schneider, D. P., Richards, G. T., Hall, P. B., et al. 2010, AJ, 139, 2360
Sesana, A. 2010, ApJ, 719, 851
Sesana, A., Haardt, F., & Madau, P. 2008, ApJ, 686, 432
Sesana, A., & Khan, F. M. 2015, MNRAS, 454, L66
Shannon, R. M., Ravi, V., Lentati, L. T., et al. 2015, Sci, 349, 1522
Shapovalova, A. I., Doroshenko, V. T., Bochkarev, N. G., et al. 2004, A&A, 422, 925
Shapovalova, A. I., Popović, L. Č., Burenkov, A. N., et al. 2010, A&A, 517, A42
Shen, Y., Brandt, W. N., Dawson, K. S., et al. 2015, ApJS, 216, 4
Shen, Y., & Ho, L. C. 2014, Natur, 513, 210
Shen, Y., Liu, X., Loeb, A., & Tremaine, S. 2013, ApJ, 775, 49
Shen, Y., & Loeb, A. 2010, ApJ, 725, 249
Shen, Y., Richards, G. T., Strauss, M. A., et al. 2011, ApJS, 194, 45
Shi, J.-M., & Krolik, J. H. 2015, ApJ, 807, 131
Simić, S., & Popović, L. Č. 2016, Ap&SS, 361, 59
Smee, S. A., Gunn, J. E., Uomoto, A., et al. 2013, AJ, 146, 32
Springel, V., Di Matteo, T., & Hernquist, L. 2005, ApJL, 620, L79
Sredzinska, J., Czerny, B., Hryniewicz, K., et al. 2016, arXiv:1602.01975
Steinhardt, C. L., Schramm, M., Silverman, J. D., et al. 2012, ApJ, 759, 24
Storchi-Bergmann, T., Nemmen da Silva, R., Eracleous, M., et al. 2003, ApJ, 598, 956
Taylor, S. R., Vallisneri, M., Ellis, J. A., et al. 2016, ApJL, 819, L6
The NANOGrav Collaboration 2016, arXiv:1602.06301
Tsalmantza, P., Decarli, R., Dotti, M., & Hogg, D. W. 2011, ApJ, 738, 20
Valtonen, M. J., Lehto, H. J., Nilsson, K., et al. 2008, Natur, 452, 851
Vasiliev, E., Antonini, F., & Merritt, D. 2015, ApJ, 810, 49
Volonteri, M., Haardt, F., & Madau, P. 2003a, ApJ, 582, 559
Volonteri, M., Madau, P., & Haardt, F. 2003b, ApJ, 593, 661
Volonteri, M., Miller, J. M., & Dotti, M. 2009, ApJL, 703, L86
Wyithe, J. S. B., & Loeb, A. 2003, ApJ, 590, 691
York, D. G., Adelman, J., Anderson, J. E., Jr., et al. 2000, AJ, 120, 1579
Yu, Q. 2002, MNRAS, 331, 935